KERNFORSCHUNGSZENTRUM

KARLSRUHE

Juni 1973 KFK 1823

Institut für Experimentelle Kernphysik

An Analytical Expression Describing the Magnetic Shielding Properties of Iron Pipes for Longitudinal Magnetic Fields

P. Hanke, W. Isenbeck, J. Moritz
K.H. Schmidt, D. Wegener

GESELLSCHAFT
FÜR
KERNFORSCHUNG M.B.H.

KARLSRUHE

KERNFORSCHUNGSZENTRUM KARLSRUHE

KFK 1823

Institut für Experimentelle Kernphysik

AN ANALYTICAL EXPRESSION DESCRIBING THE MAGNETIC SHIELDING PROPERTIES OF IRON PIPES FOR LONGITUDINAL MAGNETIC FIELDS

P. Hanke, W. Isenbeck, J. Moritz, K.H. Schmidt, D. Wegener*

Institut für Experimentelle Kernphysik der Universität und des Kernforschungszentrums Karlsruhe

Gesellschaft für Kernforschung m.b.H. Karlsruhe

* Present address: CERN (Geneva), Switzerland

ABSTRACT:

We have investigated systematically the magnetic shielding properties of iron for longitudinal fields by varying the wall thickness, length, and the diameter of the cylinder as well as the external field. An analytical expression has been derived, based on phenomenological arguments, which fits the whole data set.

ZUSAMMENFASSUNG:

Die Abschirmwirkung von Eisenzylindern für longitudinale magnetische Felder wurde systematisch untersucht. Die Abhängigkeit des Abschirmfaktors von der Länge, dem Durchmesser und der Wandstärke des Eisenzylinders wurde für verschiedene äußere Feldstärken gemessen. Die Meßdaten können mit Hilfe eines analytischen Ausdrucks beschrieben werden, der zwei anzupassende Parameter enthält.

1. INTRODUCTION:

At one interaction region of the proton Intersecting Storage Rings (ISR) at CERN |1| a multi-purpose detector is being installed, consisting basically of a large magnet with a volume of $28m^3$ filled up with proportional wire spark chambers |2|. To this basic set up further detectors are added, e.g. total absorption shower counters, Cerenkov hodoscopes and scintillation counters to allow the investigation of definite classes of reactions. All these counters will be located at places where the fringe field of the detector magnet is of the order of a few hundred Gauss.

Therefore an effective magnetic shield has to be constructed which is able to reduce by a factor of thousand the magnetic field at those places, where the photomultiplier tubes of the detectors are mounted. A cheap and versatile shield can be constructed using iron pipes of large wall thickness. They can lower the field strength inside the pipe to a value of the order of 1 Gauss, where an additional μ-metal shield can be used. The aim of the present experiment was to investigate the dependence of the shielding factor

$$S = \frac{H_e}{H_i} \qquad (1)$$

(H_e = external magnetic field, H_i = magnetic field inside of the iron pipe) on different parameters like wall thickness d, length L and outward diameter D_o of the pipe and on the strength of the external field H_e. An analytical expression has been derived which takes into account in a phenomenological way demagnetization and penetration effects of the magnetic field into the openings of the pipe. For all measurements magnetic iron (ARMCO) has been used, since it is cheap

Eingereicht am 6.April 1973

and possesses a permeability μ which is high enough to allow an effective shielding |3|.

2. EXPERIMENTAL SET UP AND RESULTS:

A longitudinal magnetic field was generated by a solenoid of 20 cm diameter and 110 cm length. The maximum magnetic flux obtainable with this apparatus was $\phi = 1.42 \cdot 10^5$ Gauss cm^2. Fig. 1 shows the variation of the field strength along the axis of the solenoid (z-axis). The region of approximatly constant magnetic field strength starts about 20 cm inside from the opening of the solenoid. The iron pipe was placed in the region of constant magnetic field. The magnetic field strength was measured by a hall probe.

The longitudinal magnetic field inside of the iron pipe has been determined as a function of the coordinate z for different choices of the geometrical parameters. In a first set of measurements the wall thickness of the iron pipe was varied while the length L and the outward diameter D_o of the pipe were kept constant. The measurements were performed at two fluxes $\phi_1 = 1.14 \cdot 10^5$ Gauss cm^2 and $\phi_2 = 0.57 \cdot 10^5$ Gauss cm^2 corresponding to external fields of $B_1 = 400$ Gauss and $B_2 = 200$ Gauss respectively. A list of the different geometrical parameters is given in table I. The results of these measurements are plotted in fig. 2 and fig. 3. All curves possess two characteristic features: an exponential decrease of the field for an increasing distance z along the axis of the iron pipe from the opening and a secondary maximum amidst the cylinder. With increasing wall thickness the field on the axis and the relative height of the secondary maximum de-

crease. A comparison of figs. 2 and 3 shows that the relative height of the secondary maximum depends strongly on the strength of the external magnetic field.

In a second set of experiments the field inside the iron pipe was measured as a function of its length L. The outer diameter D_o = 100 mm and the wall thickness d were kept constant. In fig. 4 to fig. 6 the variation of the field along the axis of the pipe is plotted for different geometrical parameters. With decreasing length L the field inside the pipe is lowered and the relative height of the secondary maximum decreases strongly. Because of the exponential penetration of the field into the iron pipe in longitudinal direction the effective length L_{eff} of the shielded region inside the iron pipe decreases too with decreasing length L. L_{eff} characterizes that part of the pipe which can be used effectivly for multiplier shielding.

We have measured that the field does not vary appreciably in a direction transverse to the longitudinal axis of the iron pipe. This is demonstrated in fig. 7 where the variation of the field in transverse direction at different values of the longitudinal coordinate z is plotted. The maximum variation of the field is less than 5%. This constancy is of fundamental importance for applications of the pipe in photomultiplier shielding.

3. INTERPRETATION OF THE RESULTS AND FIT TO THE DATA:

The shielding factor S, given by formula (1), can be separated into two parts which add reciprocally

$$\frac{1}{S(z)} = \frac{1}{S_{int}(z)} + \frac{1}{S_{ap}(z)} \qquad (2)$$

representing the contribution ($S_{ap}(z)$) of the field penetrating through the aperture of the pipe and the influence of the internal field ($S_{int}(z)$). The properties of the aperture contribution have been discussed in detail by Mager |4|, who derives the expression:

$$S_{ap}(z) = \frac{A}{\exp(-k_L \cdot z/R_i) + \exp(-k_L(L-z)/R_i)} \qquad (3)$$

where

$$A = \frac{1}{0.9}\sqrt{\frac{D_a}{L}} \qquad (4)$$

is an empirical value of the shielding factor at the end of the iron pipe |4|. It depends on the characteristic dimension of the cylinder. $R_i = D_i/2$ is the inner radius and L the length of the pipe. If the longitudinal component of the magnetic field vanishes at the internal surfaces of the pipe, k_L is given by the first zero of the spherical Bessel function of order 1:

$$k_L = 2.405 \qquad (5)$$

As shown in fig. 7 this assumption is a crude approximation. Therefore k_L will deviate from the theoretical value (5) and must be taken as a free parameter which is determined from the experimental data.

The first term $S_{int}(z)$ in (2) can be parametrized by |5|

$$S_{int}(z) = \frac{N_{ELL}}{4\pi}\left[\left(\frac{2z-L}{L}\right)^4 + k_{min}\left(1-\left(\frac{2z-L}{L}\right)^4\right)\right]\left[\frac{4\mu D_m \cdot d}{D_o^2} + \left(\frac{D_i}{D_o}\right)^2 - 1\right] + 1 \qquad (6)$$

where

$\frac{N_{ELL}}{4\pi}$ is the demagnetization factor of an ellipsoid with an excentricity

$$e = \sqrt{1 - \left(\frac{D_o}{L}\right)^2}$$

L length of the iron pipe

k_{min} empirical factor to be determined from the experimental data

$$D_m = \frac{D_o + D_i}{2}$$

D_o, D_i outer and inner diameter of the iron pipe

μ permeability

(all electromagnetic quantities are given in the gaussian system).

The expression in the first bracket gives the correction term of the demagnetization factor of an ellipsoid, which takes into account in first order approximation the differences of an iron pipe of finite length and an ellipsoid. The second bracket takes into account the differences in the magnetic flux of a full iron cylinder and an iron pipe |6|. A detailed discussion of the ansatz (6) has been given by Hanke |5|.

Up to now an unlimited flux of the external magnetic field was presupposed. Since the volume of the solenoid used in the experiments is small and the highest magnetic field is 500 Gauss the maximal flux in the solenoid is $\phi_{max} = 1.42 \cdot 10^5$ Gauss cm^2. For these parameters the flux in the iron pipe - calculated from tabulated values of μ |3| - is $6 \cdot 10^5$ Gauss cm^2. From this follows that we have to use an effective permeability μ_{eff} instead of the tabulated one, if we want to compare formula (6) with experimental data. As was shown in |5| the effective μ_{eff} and the permeability μ are connected by

$$\mu_{eff} = \mu \frac{(F_S - F_i) + \frac{\phi_{Fe}}{\phi_S} \mu \cdot F_i}{F_S} \qquad (7)$$

where

F_S cross section of the solenoid

F_i cross section of the iron pipe

ϕ_{Fe} flux in the iron at an external magnetic field B_e

$\phi_S = B_e \cdot F_S$ flux of the solenoid

$B_e = B_{Solenoid}$ in our measurements.

To compare formula (2) with the experimental data we have used μ_{eff} as a free parameter which is determined by a fit from the experimental values. The result of the fit for μ_{eff} can be compared with (7) to check that formula.

To examine formula (2) we have fitted this analytical expression to the different data sets characterized by a definite choice of geometrical and material parameters. In this fit k_L, k_{min} and μ of formulae (3) and (6) were handled as free parameters to be determined by the fit.

The fitting procedure was performed with a standard minimization program - MINUIT (CERN) -. Figs. 8 - 11 show the results of typical adjustments. The agreement between theoretical and experimental values is quite satisfactory.

To check the reliability of formulae (2), (3) and (5) one has to show that the free parameters are constants within the error limits. Fig. 12 and fig. 13 demonstrate that k_L and k_{min} fulfill this requirement. From the fits one gets the mean values

$$k_L = 1.75 \pm 0.10 \qquad (8)$$

$$k_{min} = 0.02 \pm 0.005 \qquad (9)$$

The value of k_L deviates from the theoretical one given in (5) as was predicted above.

Figs. 14 - 16 show the values of μ_{eff} as determined by the fit as a function of geometrical parameters and the external field. The theoretical prediction (7) is also shown in these figures and is in sufficient agreement with the values derived from the experiment, supporting the interpretation of the effective permeability as given in formula (7).

4. CONCLUSION:

The shielding properties of iron pipes for longitudinal magnetic fields can be described by formulae (2), (3), and (6) with two free parameters (8) and (9). If the flux of the external magnetic field is limited, formula (7) can be used to deduce the effective permeability.

REFERENCES

|1| E. Keil
Intersecting **Storage Rings**, CERN 72-14 (1972)

|2| A. Minten (editor)
The SFM facility, CERN/ISRC/71-19

|3| G.W. Elmen
Electric. Engineering 54, 1292 (1935)

|4| A. Mager
Zschr. angew. Physik 23, 381 (1967)

|5| P. Hanke
Abschirmung von Photomultipliern in starken Magnetfeldern, Staatsexamensarbeit, Universität Karlsruhe 1972

|6| A. Mager
IEEE Trans. on Magnetics, Vol. Mag-6, Nr. 1 (1970)

ACKNOWLEDGEMENT:

This work has been supported by the Bundesministerium für Forschung und Technik.

Table I:

List of the different geometrical parameters of the iron pipe used in the present experiment.

number of measure-ments	I	II	III	IV	V	VI	VII	VIII
inner diameter D_i [mm]	80	75	70	65	80	75	70	65
outer diameter D_o [mm]	100	100	100	100	100	100	100	100
length of the iron pipe L [mm]	500	500	500	500	500	500	500	500
wall thickness d [mm]	10	12.5	15	17.5	20	22.5	25	27.5

FIGURE CAPTIONS:

Fig. 1: Variation of the field strength along the axis of the solenoid.

Fig. 2, 3: Magnetic field inside of the iron pipe as a function of the coordinate z along the axis of the solenoid. Results for different wall thickness d are plotted. The flux of the solenoid is $\phi_1 = 1.14 \cdot 10^5$ Gauss cm^2 and $\phi_2 = 0.57 \cdot 10^5$ Gauss cm^2 respectively.

Fig. 4: Magnetic field strength along the axis of the iron pipe. Parameter of the curves is the length L of the pipe.
($\phi_e = 1.14 \cdot 10^5$ Gauss cm^2, d = 10 mm, D_o = 100 mm).

Fig. 5: Magnetic field strength along the axis of the iron pipe. Parameter of the curves is the length L of the pipe.
($\phi_e = 0.57 \cdot 10^5$ Gauss cm^2. d = 10 mm, D_o = 100 mm).

Fig. 6: Magnetic field strength along the axis of the iron pipe. Parameter of the curves is the length L of the iron pipe.
($\phi_e = 1.14 \cdot 10^5$ Gauss cm^2, d = 17.5mm, D_o = 100mm).

Fig. 7: Variation of the magnetic field inside of the iron pipe transverse to the longitudinal axis of the solenoid for different values of the longitudinal coordinate z.

Fig. 8-11: Comparison of theoretical and experimental values of the magnetic field inside of the iron pipe.

Fig. 12: Slope parameter k_L of the field component penetrating through the aperture of the iron pipe as determined by the fit procedure. k_L is plotted as a function of different geometrical and magnetic variables.

Fig. 13: Parameter k_{MIN}, used to describe the deviation of the demagnetization factor of an iron pipe from that one of an ellipsoid, as a function of different geometrical and magnetic variables.

Fig. 14-16: Effective permeability μ_{eff} as determined from the fit as a function of different geometrical and magnetic variables. The theoretical prediction of formula (7) is shown in the plots too.

FIG. 1

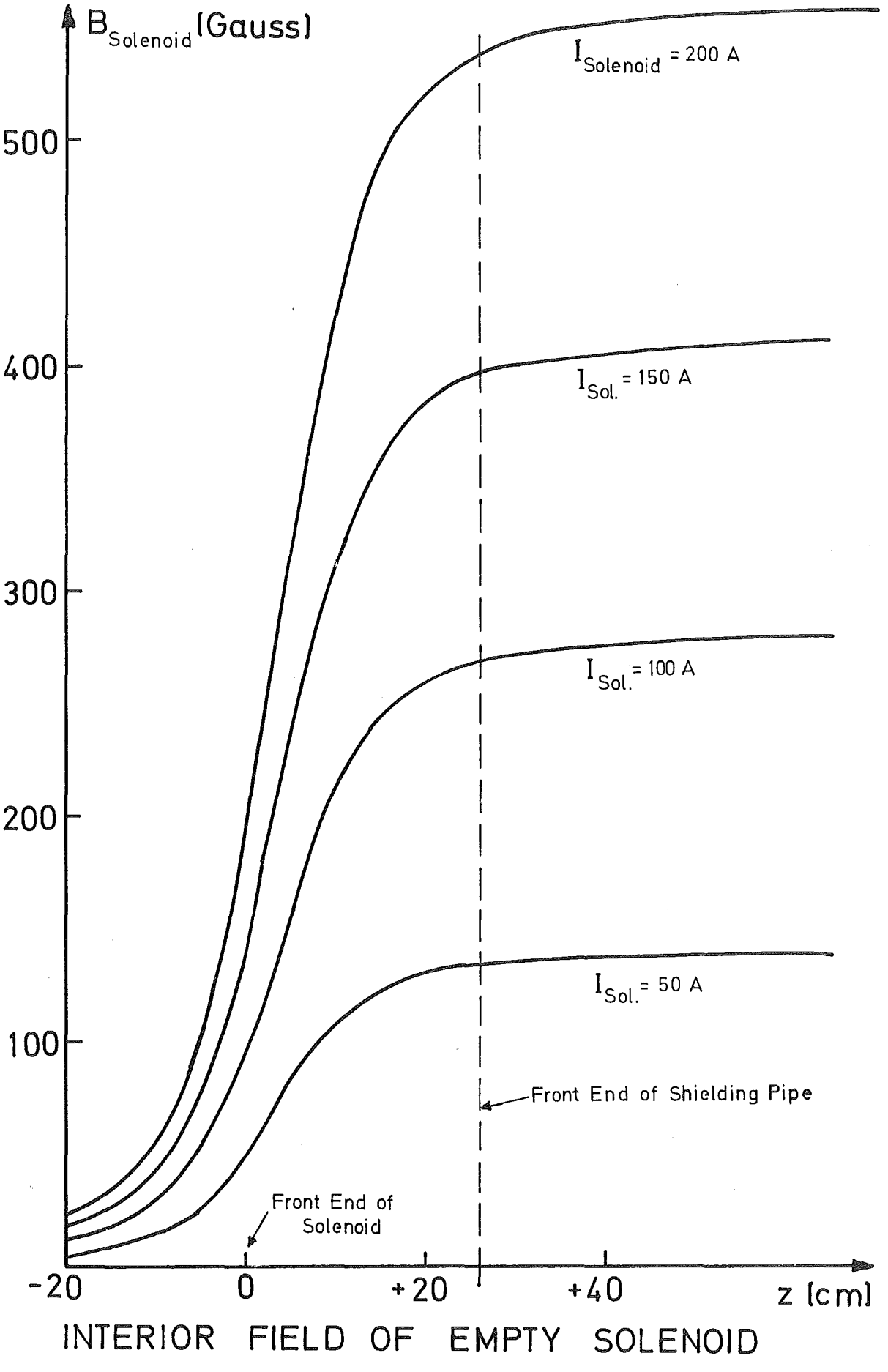

INTERIOR FIELD OF EMPTY SOLENOID

FIG. 2

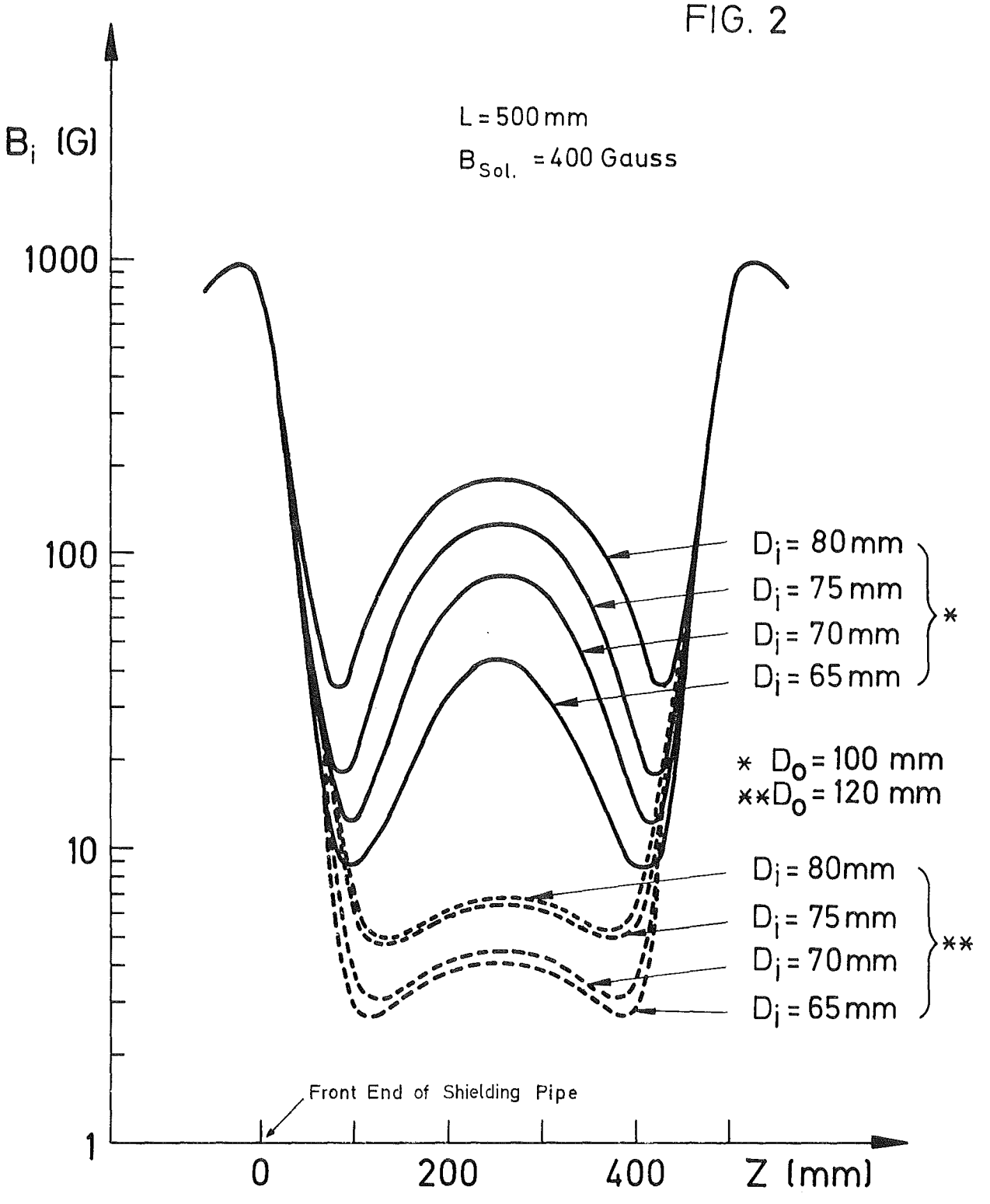

Fig. 2,3: Field Measurements for different Wall Thicknesses

FIG. 3

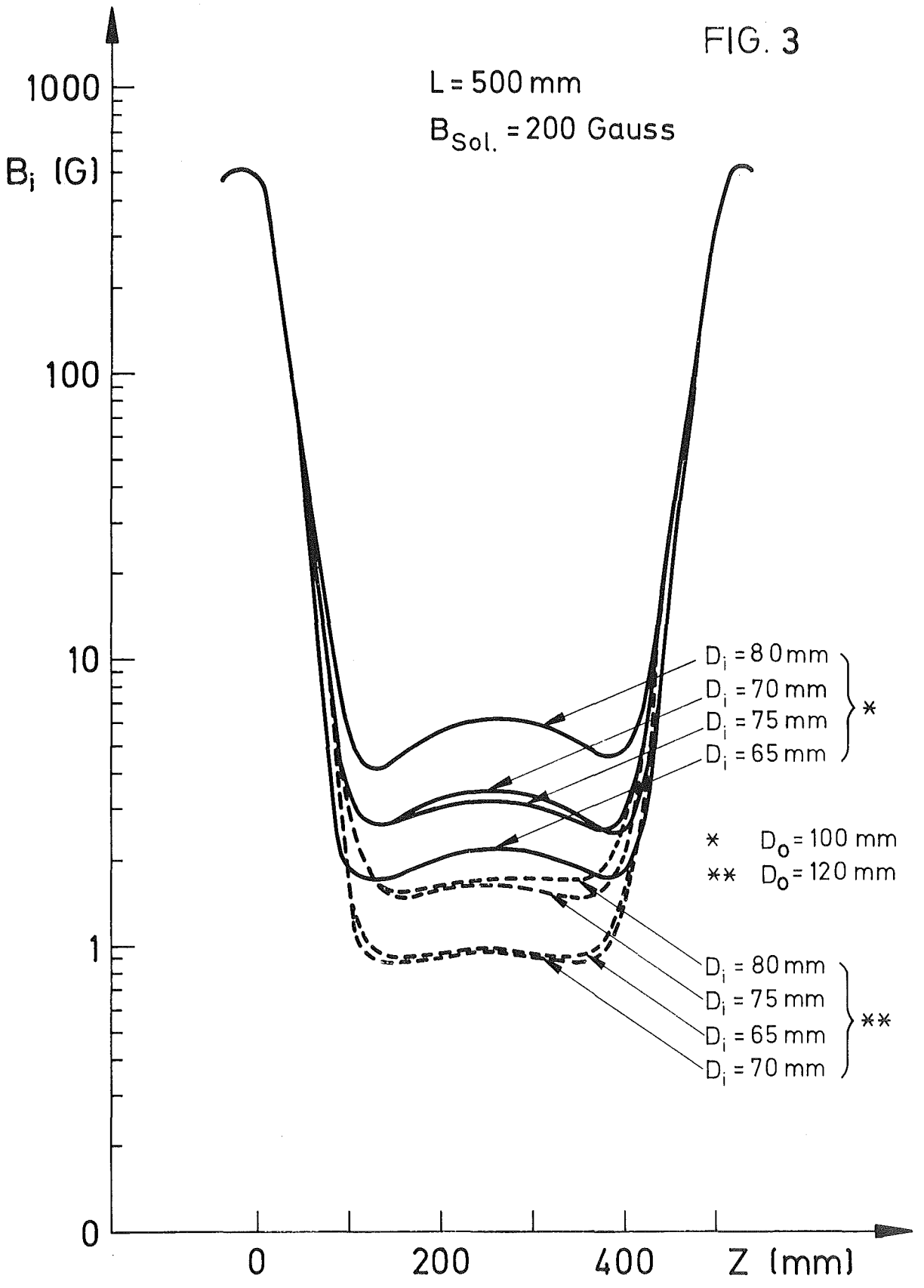
L = 500 mm
$B_{Sol.}$ = 200 Gauss
1000
B_i (G)
100
10
1
0
0
200
400
Z (mm)
D_i = 80 mm
D_i = 70 mm
D_i = 75 mm
D_i = 65 mm
*
* D_o = 100 mm
** D_o = 120 mm
D_i = 80 mm
D_i = 75 mm
D_i = 65 mm
D_i = 70 mm
**

FIG. 4

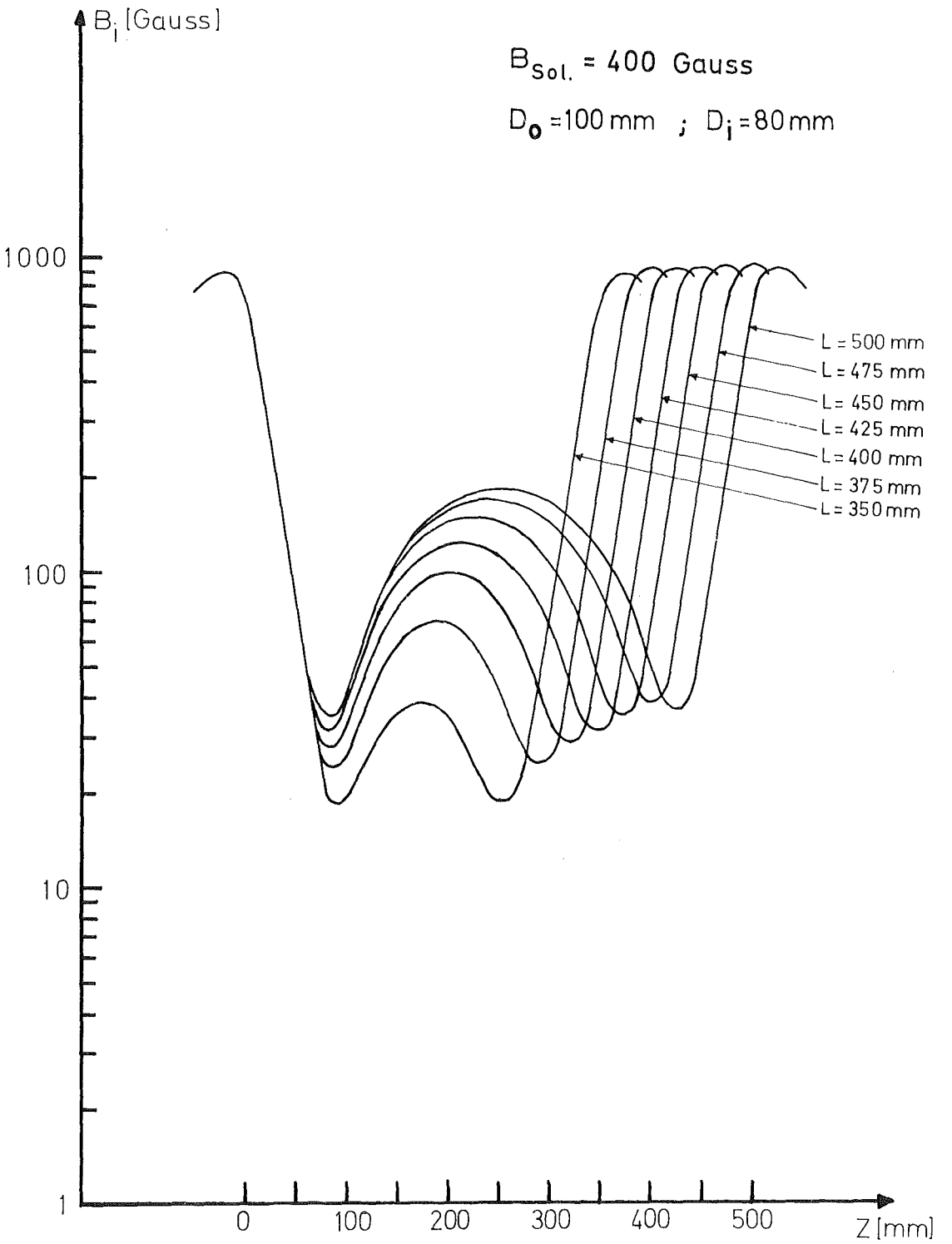

Fig. 4,5: Field Measurements for different Tube Lengths

FIG. 5

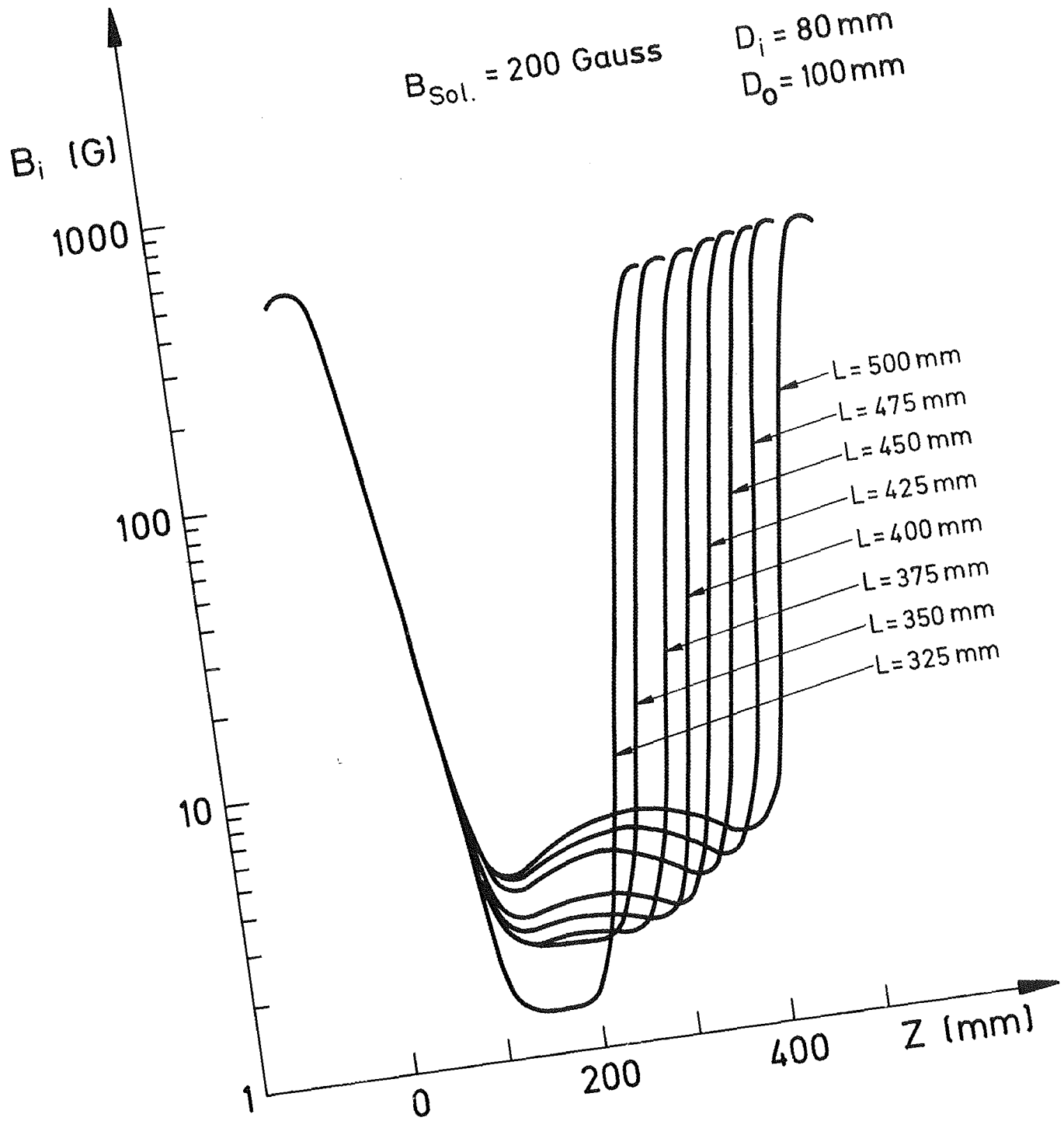
$B_{Sol.}$ = 200 Gauss
D_i = 80 mm
D_o = 100 mm
B_i (G)
1000
100
10
1
0
200
400
Z (mm)
L = 500 mm
L = 475 mm
L = 450 mm
L = 425 mm
L = 400 mm
L = 375 mm
L = 350 mm
L = 325 mm

FIG. 6

$B_{Solenoid}$ = 400 Gauss

D_o = 100 mm

D_i = 65 mm

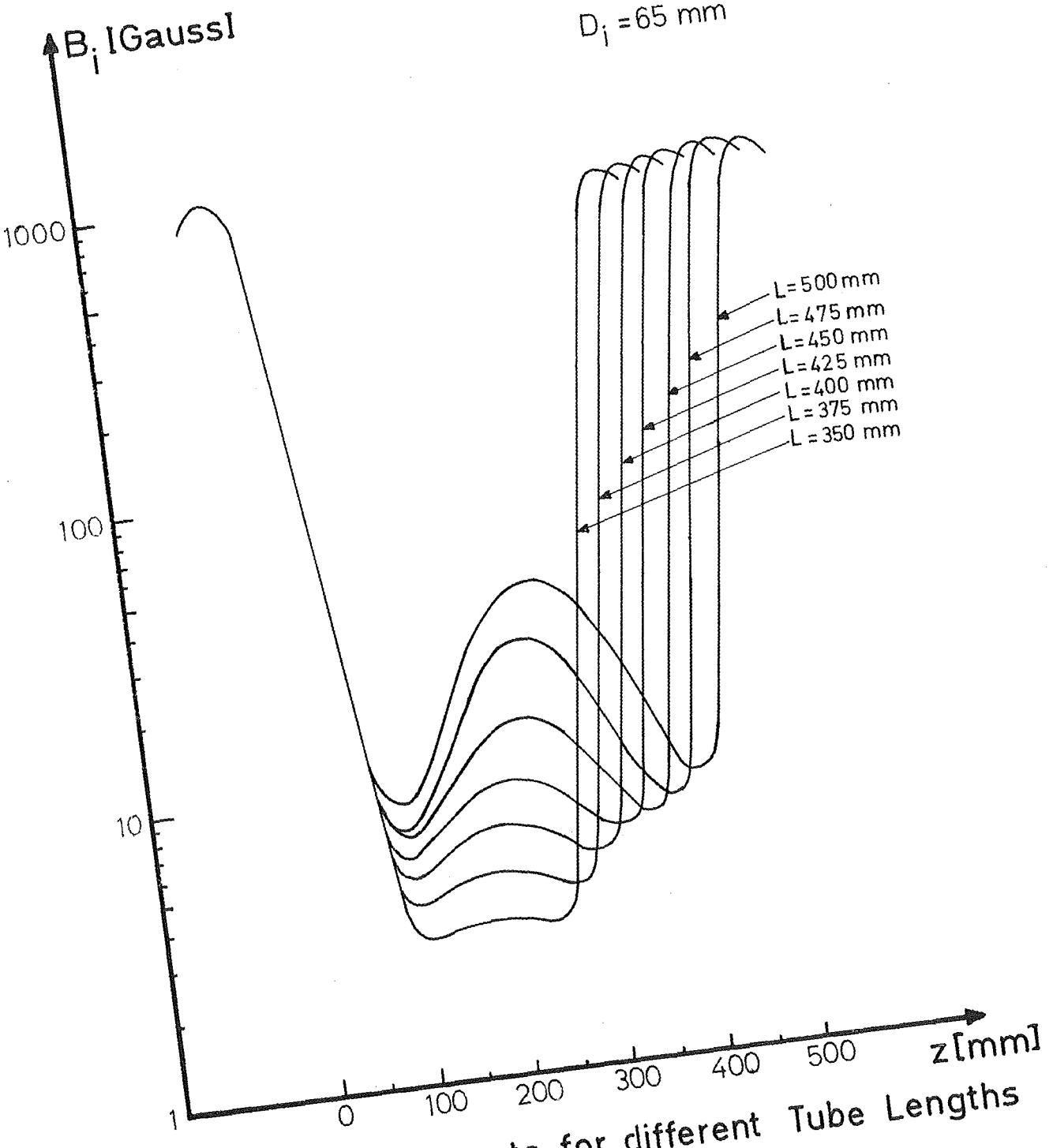

Field Measurements for different Tube Lengths

Fig. 7

D_o=120 mm ; D_i = 65 mm ; L =500 mm

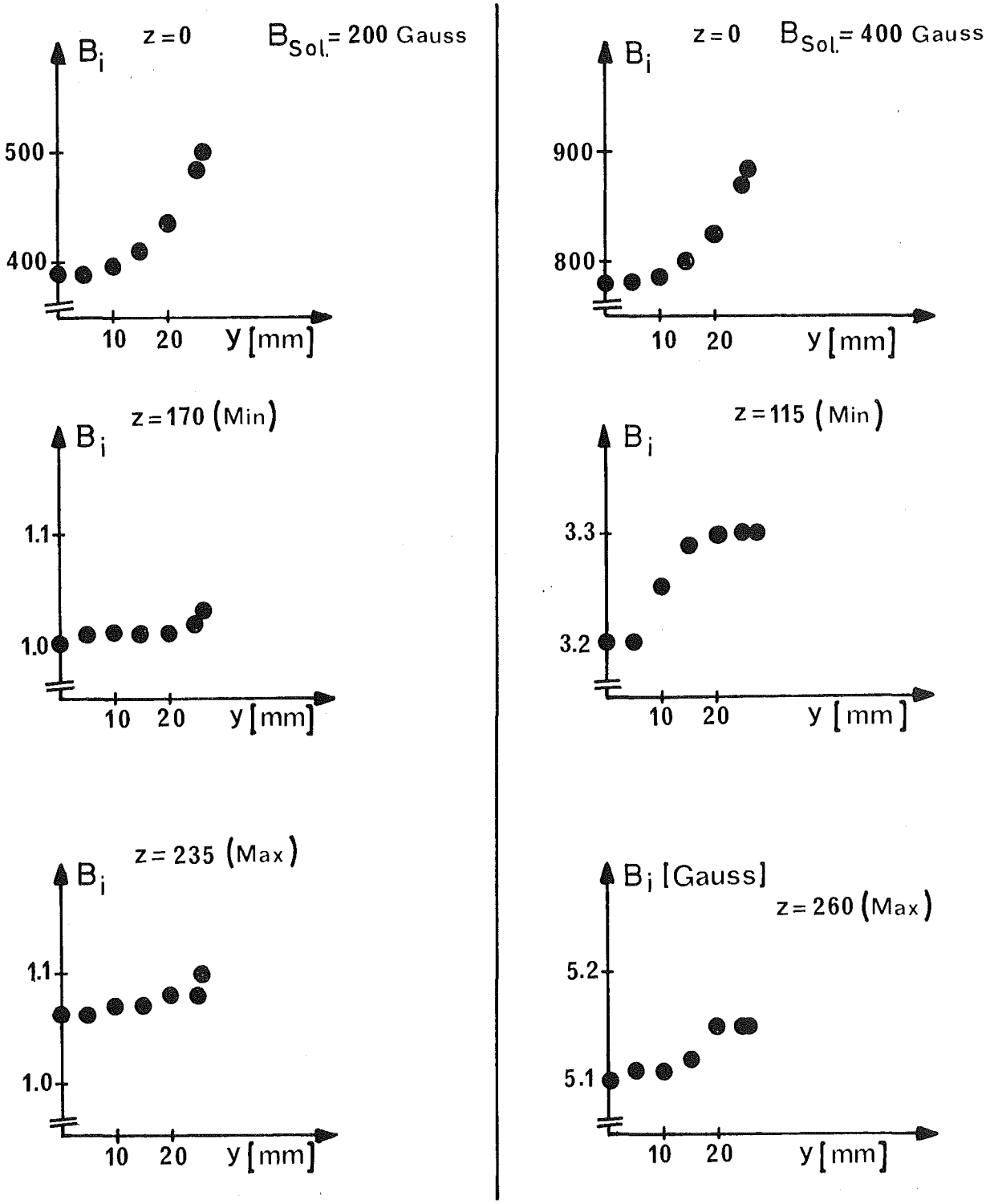

Longitudinal Field off Axis at 3 Locations

FIG. 8

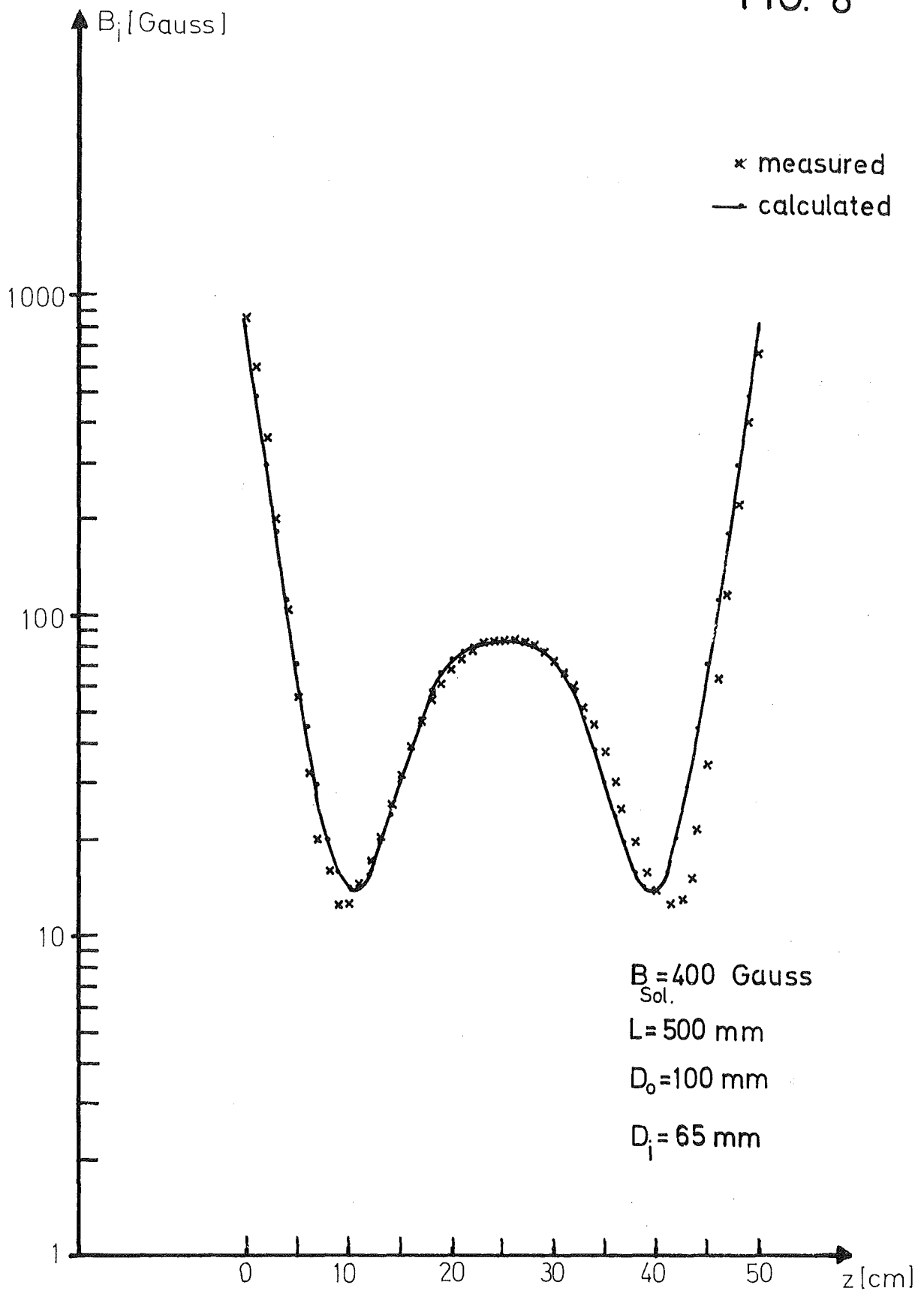

Fig. 8 - 11: Comparison of Calculation and Measurement

FIG. 9

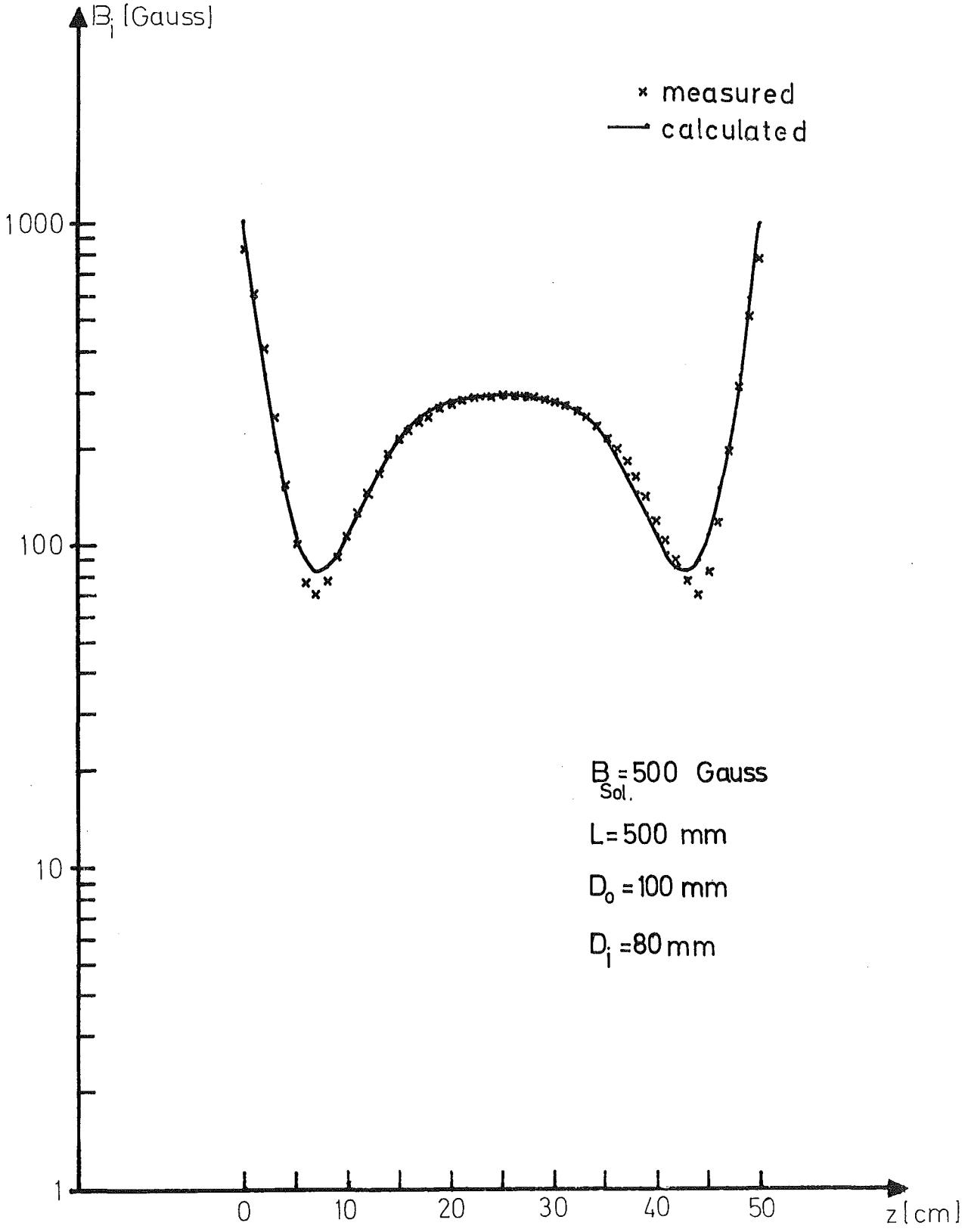
B_i [Gauss]
× measured
calculated
1000
100
10
1
0
10
20
30
40
50
z [cm]
$B_{Sol.}$ = 500 Gauss
L = 500 mm
D_o = 100 mm
D_i = 80 mm

FIG. 10

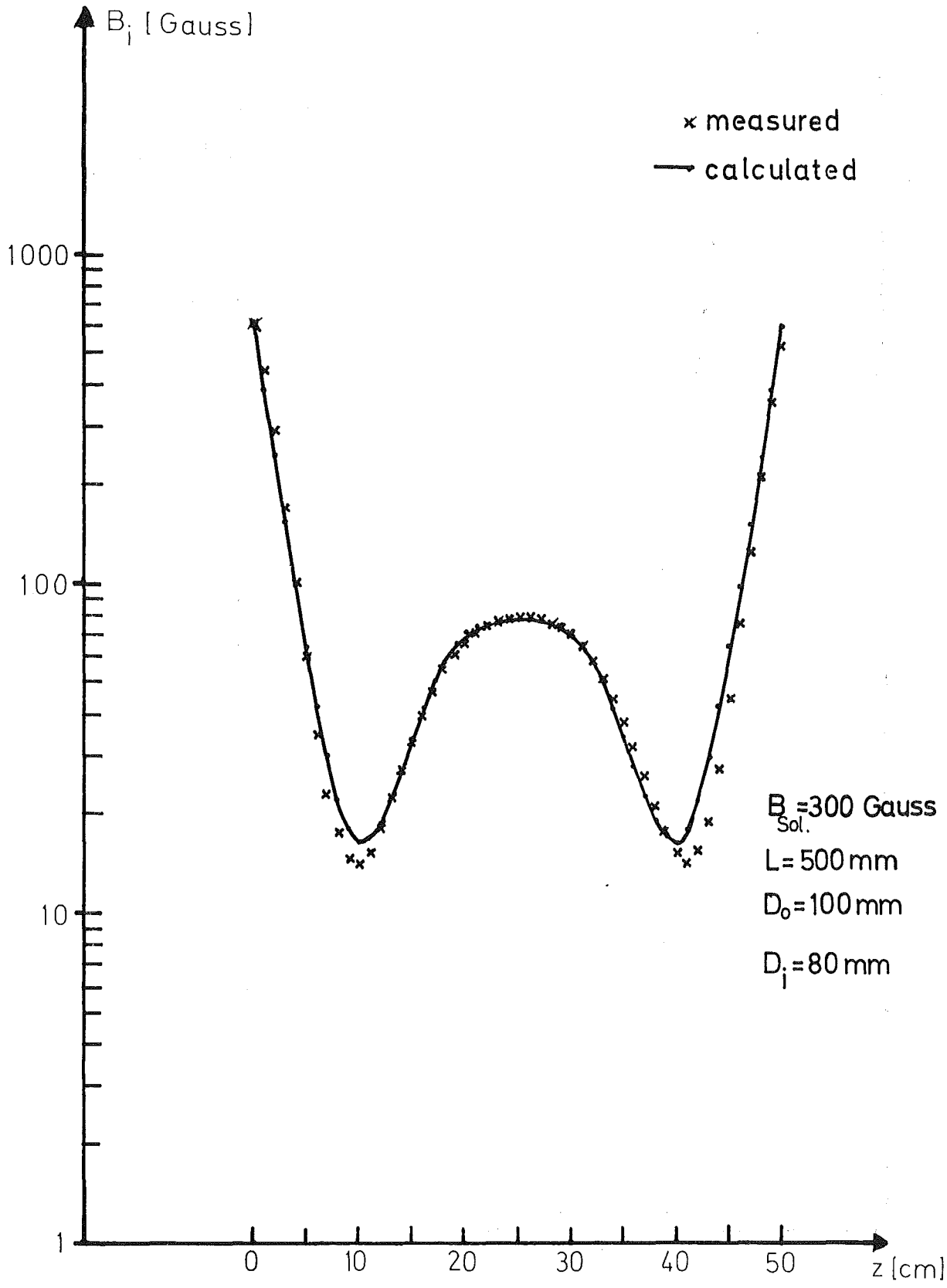
B_i [Gauss]
× measured
calculated
1000
100
10
1
0
10
20
30
40
50
z [cm]
$B_{Sol.}$ = 300 Gauss
L = 500 mm
D_o = 100 mm
D_i = 80 mm

FIG. 11

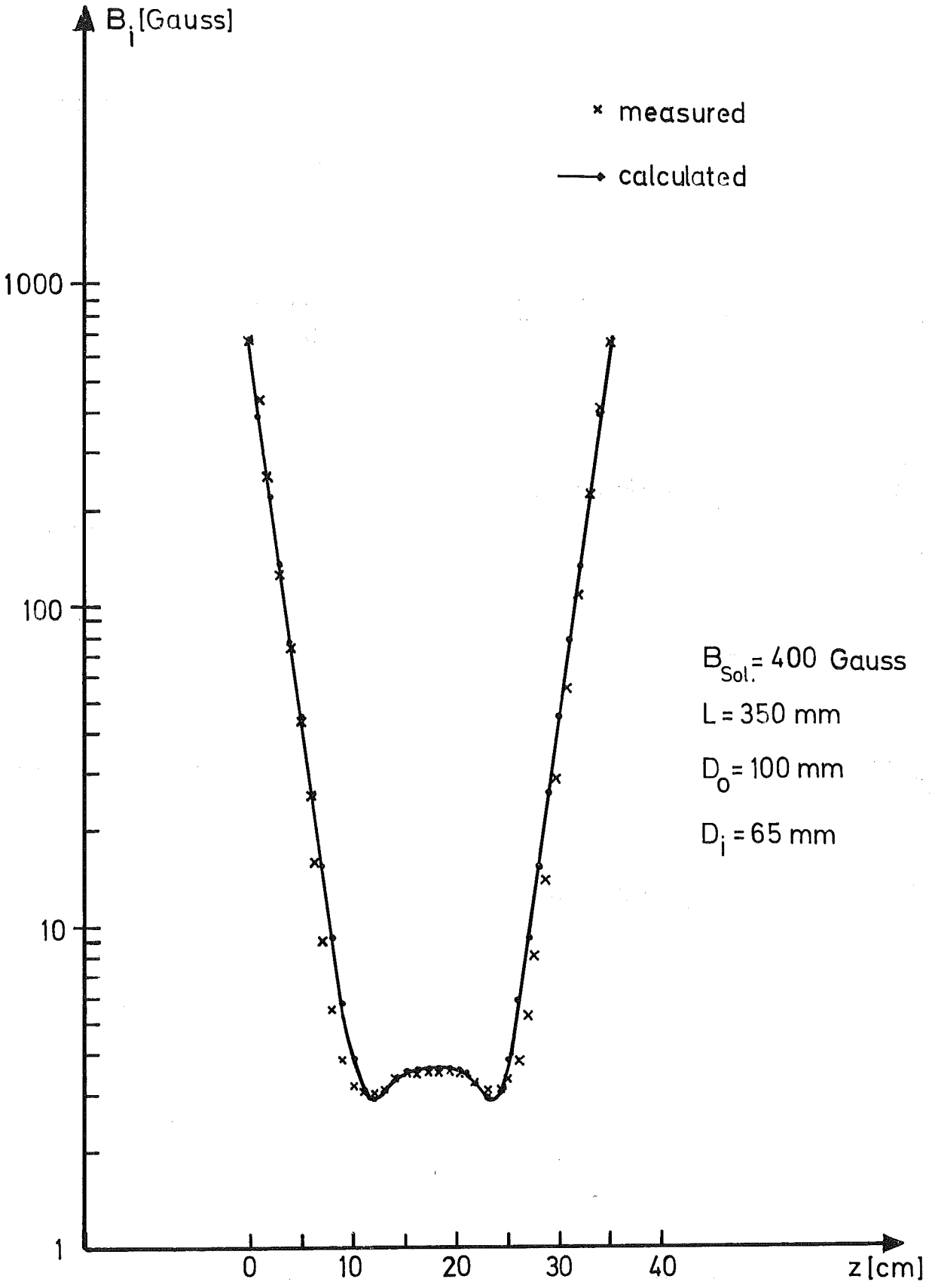
B_i [Gauss]
× measured
calculated
1000
100
10
1
0
10
20
30
40
z [cm]
$B_{Sol.}$ = 400 Gauss
L = 350 mm
D_o = 100 mm
D_i = 65 mm

FIG. 12

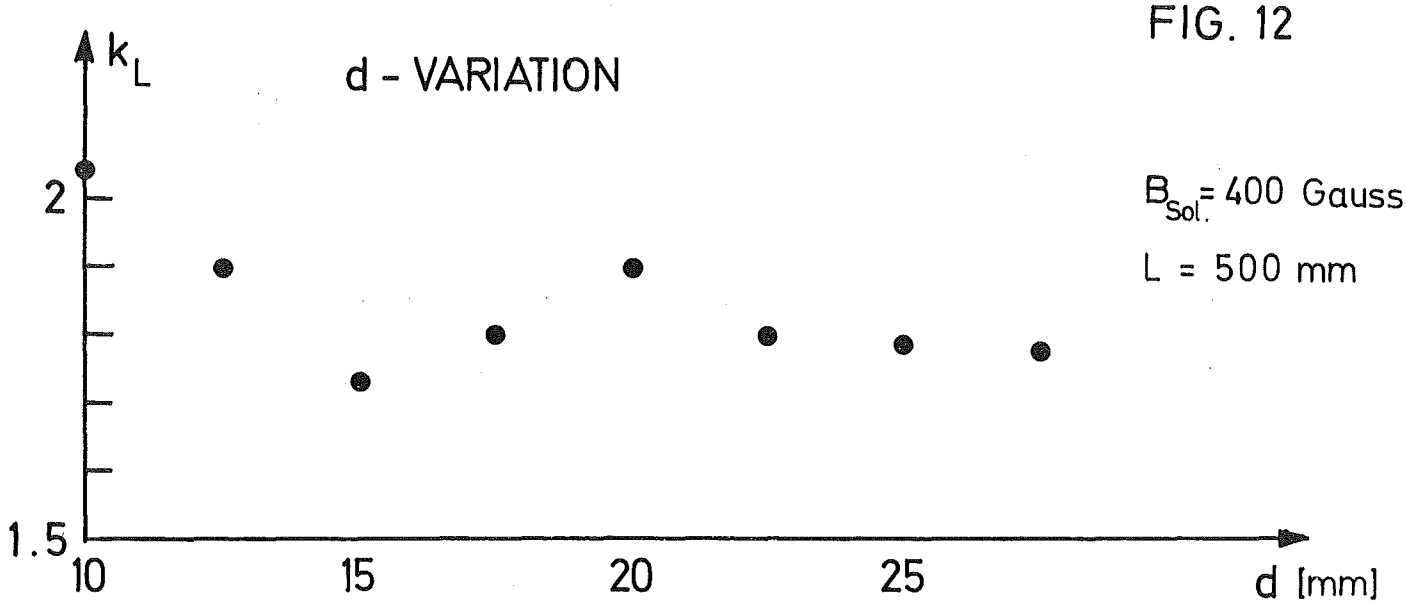
k_L
d - VARIATION
$B_{Sol.}$ = 400 Gauss
L = 500 mm
2
1.5
10
15
20
25
d [mm]

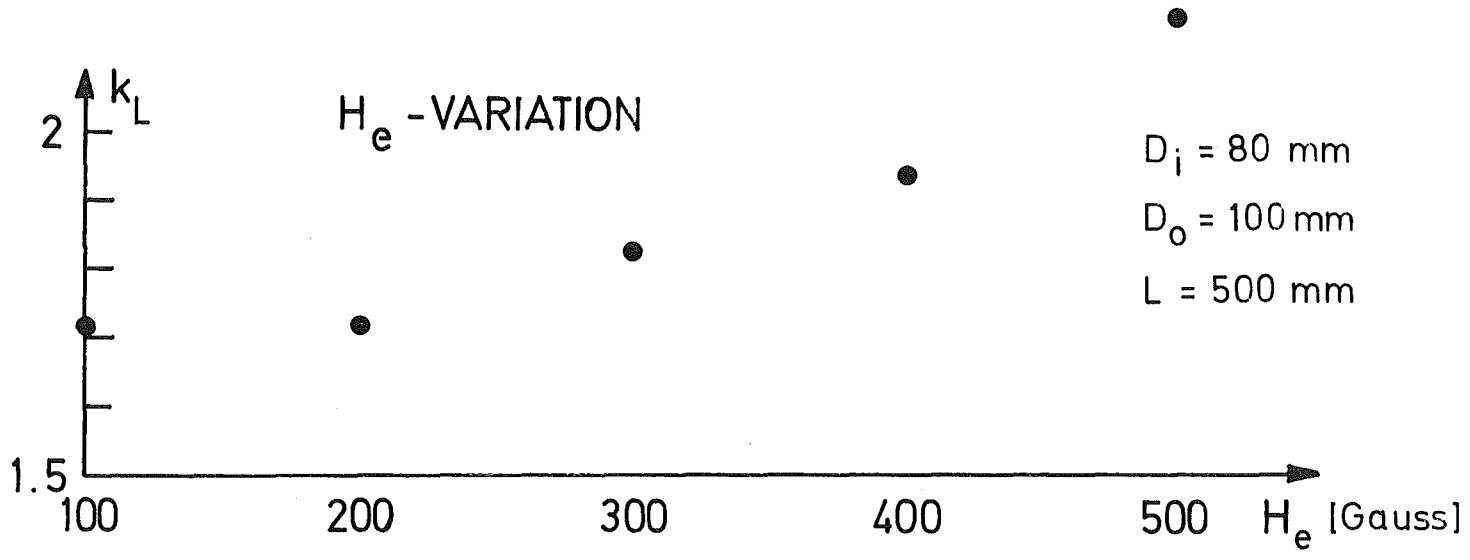
k_L
H_e - VARIATION
D_i = 80 mm
D_o = 100 mm
L = 500 mm
2
1.5
100
200
300
400
500
H_e [Gauss]

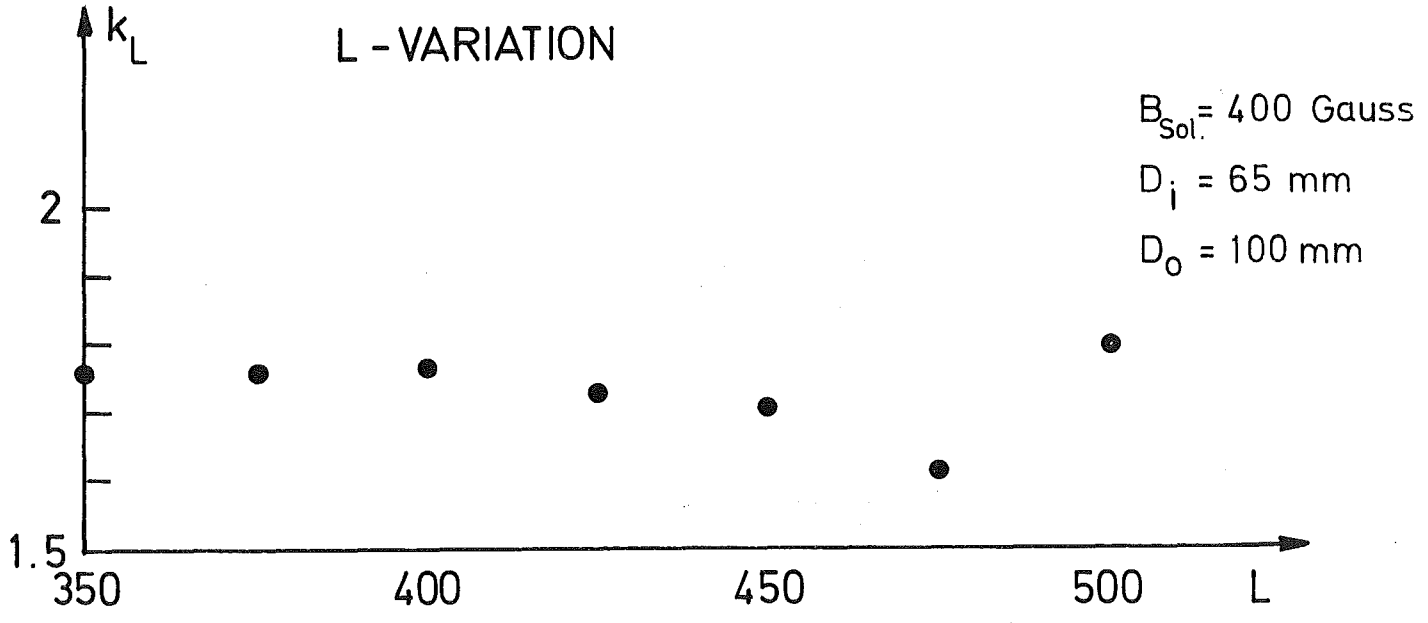
k_L
L - VARIATION
$B_{Sol.}$ = 400 Gauss
D_i = 65 mm
D_o = 100 mm
2
1.5
350
400
450
500
L

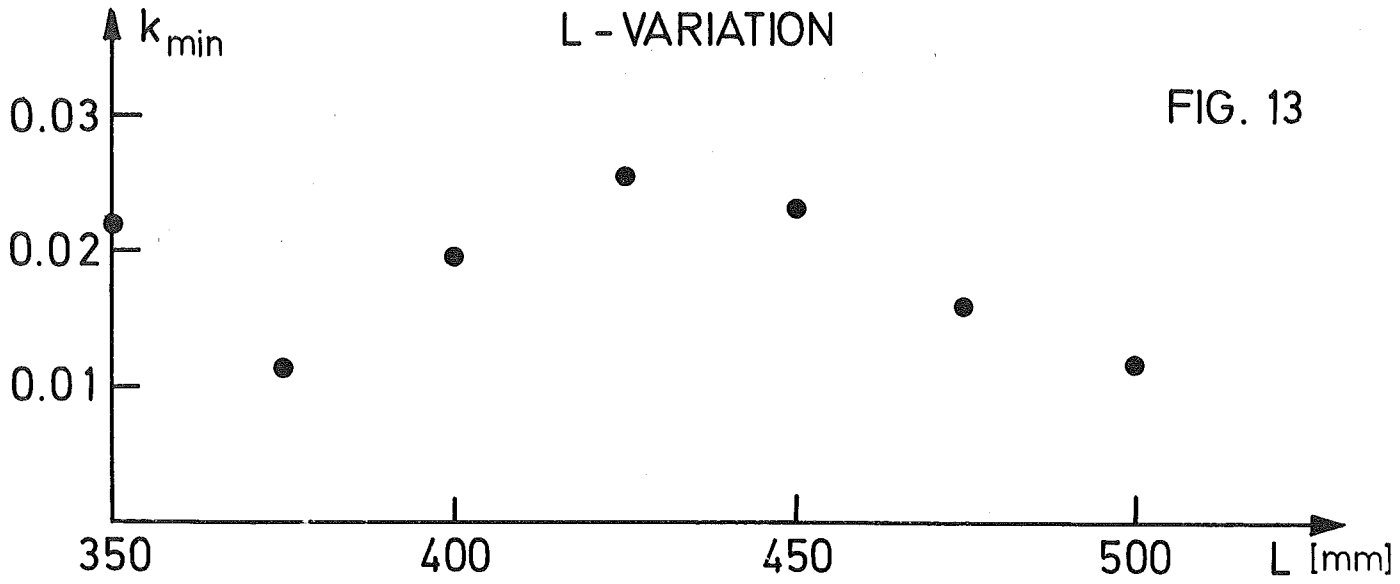
L - VARIATION
k_{min}
0.03
0.02
0.01
350
400
450
500
L [mm]

FIG. 13

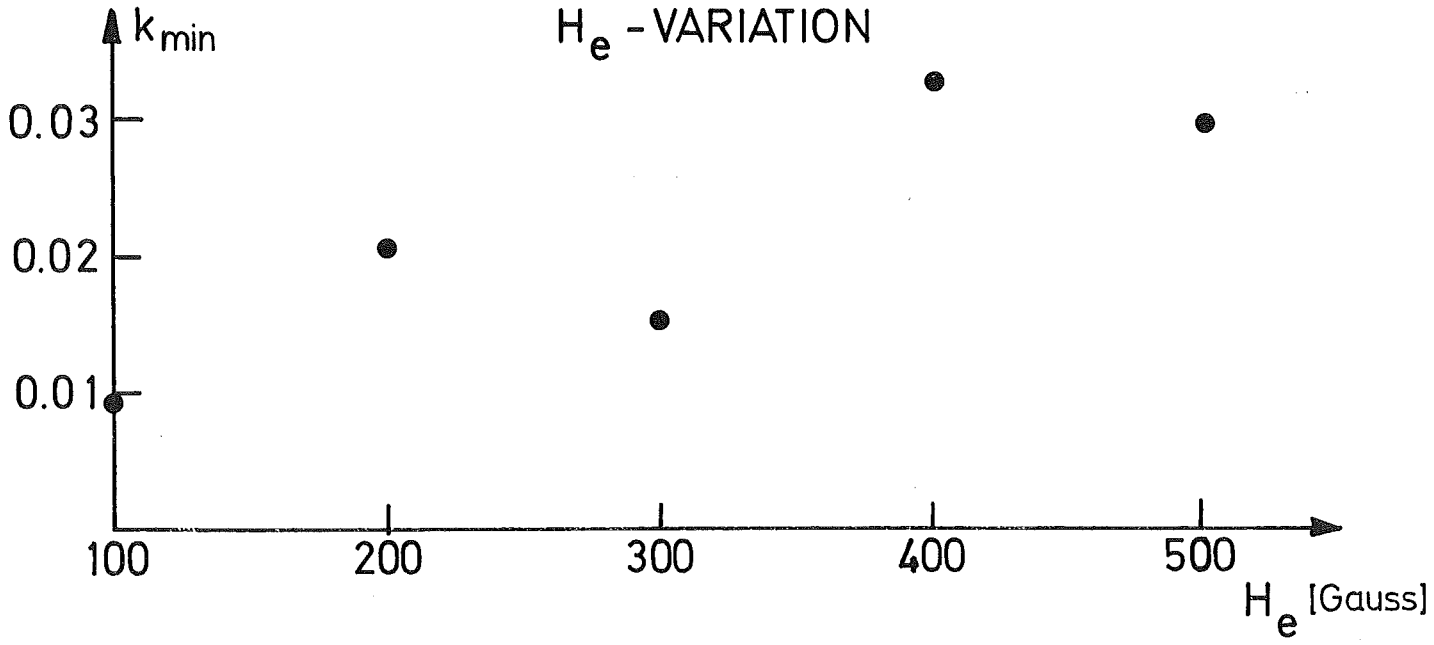
H_e - VARIATION
k_{min}
0.03
0.02
0.01
100
200
300
400
500
H_e [Gauss]

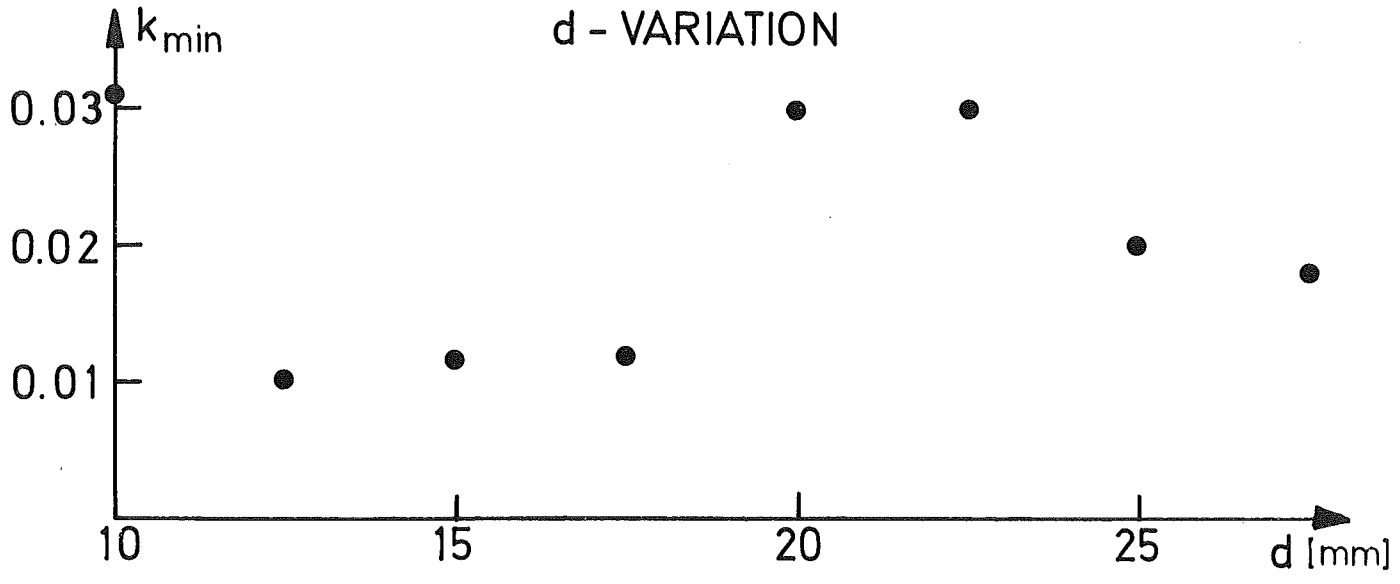
d - VARIATION
k_{min}
0.03
0.02
0.01
10
15
20
25
d [mm]

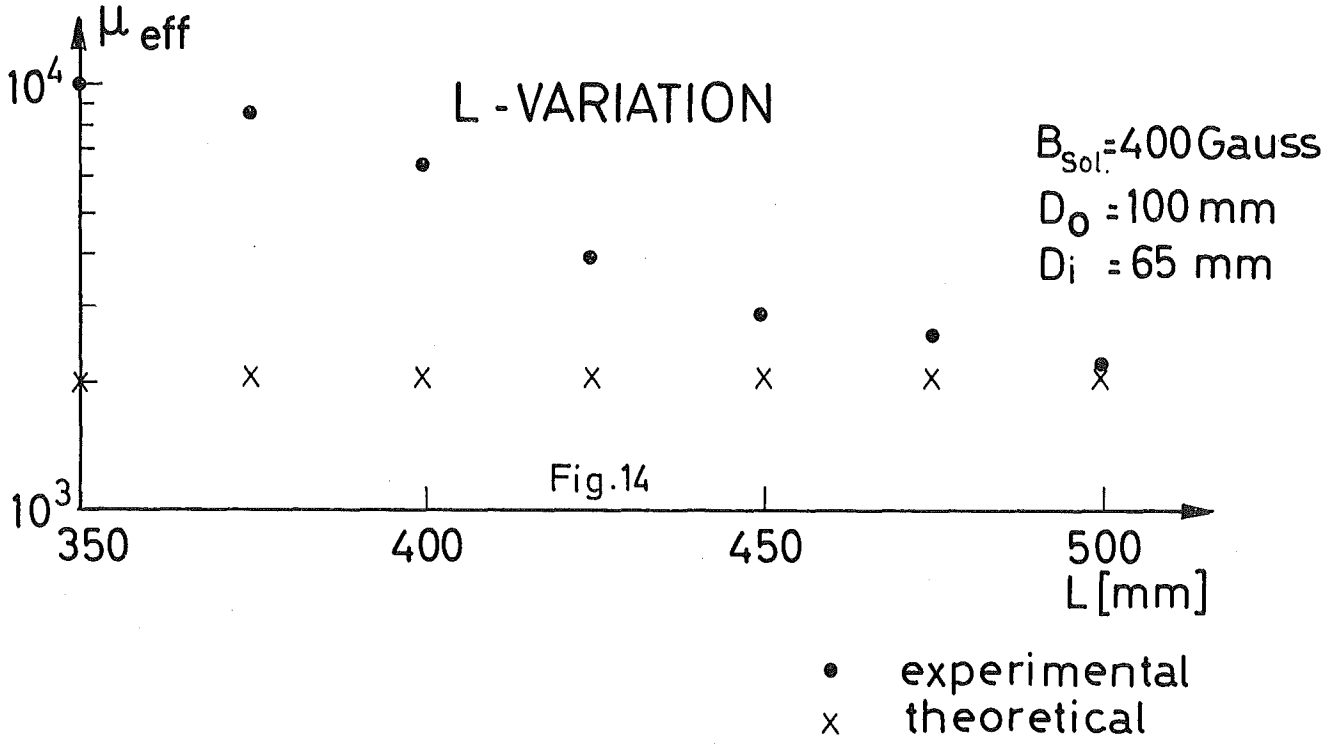
μ eff
10^4
10^3
L - VARIATION
B_Sol.=400 Gauss
D_o = 100 mm
D_i = 65 mm
350
400
450
500
L [mm]
experimental
theoretical

Fig.14

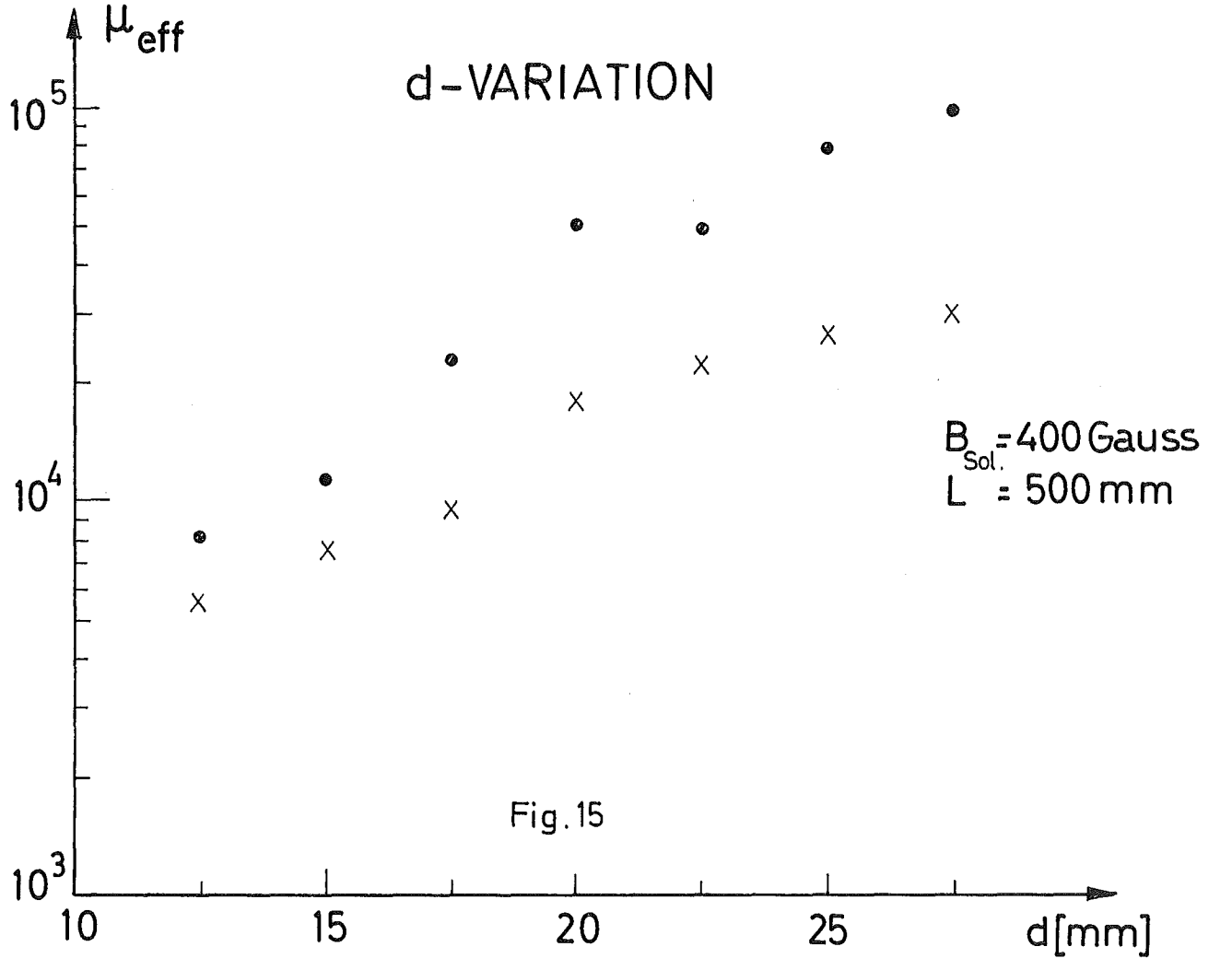
μ_eff
10^5
10^4
10^3
d - VARIATION
B_Sol.=400 Gauss
L = 500 mm
10
15
20
25
d[mm]

Fig.15

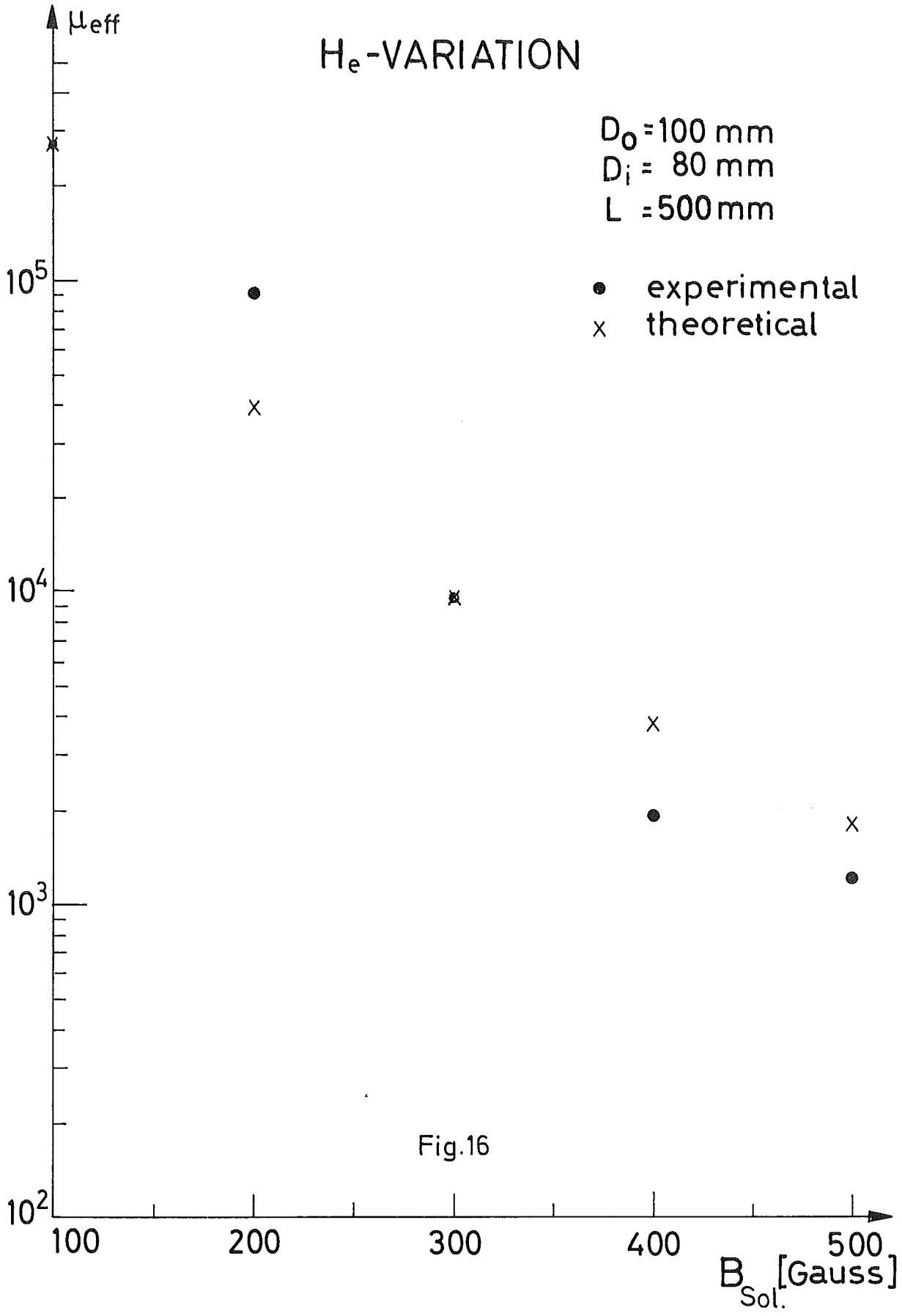
μeff
He-VARIATION
D0 = 100 mm
Di = 80 mm
L = 500 mm
experimental
theoretical
10^5
10^4
10^3
10^2
100
200
300
400
500
B Sol. [Gauss]

Fig.16